Published in final edited form as:
Dev Dyn. 2010 October ; 239(10): 2659–2673. doi:10.1002/dvdy.22405.

Expression, functional and structural analysis of proteins critical for otoconia development

Yinfang Xu[1,*], **Hui Zhang**[1,*], **Hua Yang**[1,3], **Xing Zhao**[1], **Sándor Lovas**[2], and **Yunxia (Yesha) Wang Lundberg**[1,#]

[1]Vestibular Neurogenetics Laboratory, Boys Town National Research Hospital, 555 N. 30th St., Omaha, NE 68131, USA

[2]Department of Biomedical Sciences, Creighton University, 2500 California Plaza, Omaha, NE 68178

Abstract

Otoconia, developed during late gestation and perinatal stages, couple mechanic force to the sensory hair cells in the vestibule for motion detection and bodily balance. In the present work, we have investigated whether compensatory deposition of another protein(s) may have taken place to partially alleviate the detrimental effects of Oc90 deletion by analyzing a comprehensive list of plausible candidates, and have found a drastic increase in the deposition of Sparc-like 1 (aka Sc1 or hevin) in Oc90 null vs. wt otoconia. We show that such up-regulation is specific to Sc1, and that stable transfection of Oc90 and Sc1 full-length expression constructs in NIH/3T3 cells indeed promotes matrix calcification. Analysis and modeling of Oc90 and Sc1 protein structures show common features that may be critical requirements for the otoconial matrix backbone protein. Such information will serve as the foundation for future regenerative purposes.

Keywords

Oc90; Sc1; Sparc; otoconia; biomineralization/calcification; protein homology modeling

Introduction

Otoconia are bio-crystals composed of $CaCO_3$ and proteins, and couple mechanic force generated from linear acceleration and gravity to the macular sensory hair cells in the utricle and saccule of the inner ear for motion sensing, spatial orientation and bodily balance. Unlike the inorganic counterpart, the shape, size and organization of $CaCO_3$ crystallites in otoconia and otoliths are strictly controlled by an organic matrix composed of proteins and proteoglycans. Despite the common $CaCO_3$ component, otoconia/otoliths from animals of different evolutionary levels have various morphologies and crystalline structures due to different protein compositions, further suggesting the importance of otoconins in otoconia development. More importantly, as the endolymph has an extremely low Ca^{2+} concentration, otoconial proteins (collectively called otoconins) presumably are essential for $CaCO_3$ crystal formation.

[#]Corresponding author: Yunxia (Yesha) Wang Lundberg, Ph. D., Vestibular Neurogenetics Laboratory, Boys Town National Research Hospital, 555 N. 30th St., Omaha, NE 68131, Ph : 1-402-498-6735, Fax : 1-402-498-6351, yesha.lundberg@boystown.org.
[3]Present address: School of Life Science and Technology, Tongji University, Shanghai, China 200092
[*]Y.X. and H.Z. contributed equally to the work.

To date, as many as 5 component proteins have been identified from murine otoconia and 8 from fish otoliths. In mice, these include Oc90 (Verpy et al. 1999;Wang et al. 1998), otolin-1 (Zhao et al. 2007), osteopontin (Sakagami 2000;Takemura et al. 1994;Zhao et al. 2008a), fetuin-A (aka countertrypin) (Zhao et al. 2007;Thalmann et al. 2006;Zhao et al. 2007), and possibly Sparc-like 1 (secreted protein acidic and rich in cysteine, aka Sc1) (Thalmann et al. 2006). In fish, the known component proteins are otolith matrix protein (OMP) (Murayama et al. 2000;Murayama et al. 2002), otolin-1 (Murayama et al. 2002;Davis et al. 1995;Murayama et al. 2002), Starmaker (Sollner et al. 2003), matrix macromolecule-64 (Tohse et al. 2008), Otoc1 (zOc90) (Petko et al. 2008;Petko et al. 2008), Sparc, precerebellin-like protein (Cblnl) and neuroserpin (Kang et al. 2008). Knockdown of OMP, otolin-1, Starmaker, Sparc and Otoc1 lead to various abnormalities in zebrafish otolith growth (Kang et al. 2008;Murayama et al. 2004;Murayama et al. 2005;Sollner et al. 2003). In the absence of the predominant crystal protein otoconin-90 (Oc90), the otoconia organic matrix is nearly absent and the efficiency of crystal formation is reduced by 50%. In addition, the largely inorganic crystallites form aggregates with abnormal morphologies and sizes (Zhao et al. 2007). These facts suggest that the organic matrix of otoconia/otoliths serves as a framework for the inorganic $CaCO_3$ crystallites to deposit and grow. Furthermore, recent studies have demonstrated that zebrafish OMP and mouse Oc90 are required for the deposition of otolin-1 (Murayama et al. 2005;Zhao et al. 2007). Like otolin-1, the recently identified Cblnl (Kang et al. 2008) has a C1q domain. Therefore, some of these components may interact with each other to form the organic framework for efficient crystallization.

We have previously demonstrated that otolin was absent (or below the detection level) in Oc90 null crystals, whereas fetuin-A and osteopontin were present (Zhao et al. 2007). To further test whether there are compensatory events that have mitigated the detrimental effects of Oc90 deletion and to identify additional remnant component(s) in Oc90 null otoconia, we analyzed the other probable proteins, including Sparc and Sc1, in the present study. Given the shared protein components (e.g. osteopontin, fetuin-A, collagen and collagen-like proteins) and similar ultra-structures between otoconia and bone crystals, we also analyzed a number of important bone matrix proteins and proteoglycans to see if they are present in wt otoconia and if they are up-regulated in the Oc90 null vestibule.

Results

Compensatory deposition of Sparc-like (Sc1) in Oc90 null otoconia

In order to identify possible compensatory events that may have partially alleviated the detrimental effects of Oc90 deletion on otoconia formation, we analyzed a number of candidate matrix proteins and proteoglycans to see if they are present in wt otoconia and if their deposition is altered in Oc90 null otoconia at perinatal and postnatal stages. The low organic composition of Oc90 null otoconia (Zhao et al. 2007) makes it infeasible to collect sufficient material for mass spectrometric analysis; therefore, we used the extremely sensitive fluorescent immunostaining and Western blotting methods and tested candidate proteins. Figures 1B, 1D, 1F show a massive staining of Sc1 protein in the null otoconia (labeled as “O”) at E18.5, P0 and P21, whereas faint staining in wt otoconia was slightly visible only under the microscope but not in the photographs. Figures 1G and 1H show negative controls using the non-immune serum. This trend was consistent in different sections of each animal and in different individuals/ages.

To ensure that the observed higher amount of Sc1 protein in Oc90 null otoconia was not simply the result of increased antigen accessibility in the null tissue, we performed semi-quantitative Western blotting of otoconia extracts from P2–3 wt and null mice (Figure 2A). We compared the differences in Sc1 quantity in two groups where two different protein

ratios from wt vs. null were loaded: 6:6 μg and 6:2 μg (wt:null) of total protein. This is equivalent to otoconia from 1 wt versus 3 null mice in the first group, and 1 wt versus 1 null mouse in the 2nd group. Only the result from the 2nd group is shown in Figure 2A. In both groups, null otoconia had a single intense band in the size of approximately ~130–140 kD (Figure 2A, "Null O") that was likely dimerized Sc1, whose predicted unmodified molecular weight is 72 kD. In contrast, wt otoconia did not show any band; after a much pro-longed exposure, the lane had a faint band near ~130–140 kD. Thus, the blotting results confirmed the tremendous increase in Sc1 deposition in Oc90 null otoconia. A Sc1 dimer with a similar size range has been detected by Western blotting of tissues and cell cultures in a number of reports (Girard and Springer 1996;Claeskens et al. 2000) (also Figure 6F).

To examine whether this up-regulation was due to an increase in gene transcription, we performed qRT-PCR analysis of dissected utricular and saccular epithelia from wt and null mice. The elevation of *Sc1* transcript was significant in the null epithelia compared to wt tissues at E17.5 ($P<0.01$, n=3, indicated by ** in Figure 2B) but not at P0 (Figure 2B). The neonatal (P0) *Sc1* transcript level (relative to β-actin) was 50% and 21% higher than that at embryonic (E17.5) stages in wt and null epithelia, respectively ($P<0.001$ and 0.01, respectively, n=3, indicated by ## and ### in Figure 2B).

The deposition of Sparc itself was also slightly increased in the null otoconia at neonatal and postnatal ages examined (Figures 3A–3C). Likewise, staining in wt otoconia was only slightly visible under the microscope but not in the photographs. This increase of Sparc in Oc90 null otoconia was also confirmed by Western blotting of the same amount of otoconia extracts (approx. 7 μg total protein) from P15 mice ("WT O" and "Null O" in Figure 3C). However, the *Sparc* transcript level (relative to β-*actin*) in the null utricular and saccular epithelia was not higher than that in wt tissues (Figure 3D). In both genotypes, *Sparc* expression levels showed a reducing trend with age ($P<0.001$, n=4, P0 vs. E17.5, indicated by ### in Figure 3D). The expression sites of both Sc1 and Sparc remained unaltered in Oc90 null vs. wt epithelia. In both genotypes, both proteins were detected in hair cells, supporting cells and sub-regions of the roof (Figures 1 and 3). In addition, Sc1 was also present in nerve fibers and Sparc in fibrocytes and cartilage (not shown). The presently observed immunostaining patterns of Sc1 and Sparc in the vestibule are consistent with reported expression of *Sc1* and *Sparc* mRNA detected by *in situ* hybridization in the rat (Mothe and Brown 2001b), and *Sparc* mRNA and protein detected by *in situ* hybridization and immunofluorescence in the vestibule of the zebrafish (Kang et al. 2008). Specifically, in the rat, *Sc1* mRNA was highly expressed in the spiral ganglion, fibrocytes of the spiral ligament and marginal cells of the stria vascularis; whereas *Sparc* mRNA was detected in the temporal bone, cartilage, spiral limbus, fibrocytes of the spiral ligament and deiter's cells. In the zebrafish, *Sparc* mRNA and protein were detected in both hair and supporting cells of the vestibular macula (Kang et al. 2008).

Our data suggest a developmental role of these two proteins in the vestibule. Such a role has been reported in the brain and the cochlea (Mendis et al. 1996a;Mendis et al. 1996b;Mothe and Brown 2001a;Mothe and Brown 2001b). The proteins may also play a role in neurite growth, particularly following injury (Mendis et al. 1996a;Pollerberg and Mack 1994). Currently it is not clear what upstream genes regulate the expression of these proteins. The small or no difference in Sc1 and Sparc mRNA levels between age-matched Oc90 wt and null tissues suggest that the increase in Sc1 and Sparc in Oc90 null otoconia most likely have come from protein recruitment, therefore, we analyzed below possible common structural features that may underlie such compensatory recruitment after we tested whether such increase is specific to Sc1/Sparc.

Analysis of additional candidates that may be present in Oc90 wt or null otoconia

We have previously shown that fetuine-A and osteopontin remain unchanged or at most slightly elevated in Oc90 null crystals (Zhao et al. 2007), and that these two proteins are unlikely to play important roles in otoconia formation (Pollerberg and Mack 1994;Zhao et al. 2008b) (also see Discussion). Here we analyzed other inner ear and calcified matrix proteins including proteoglycans, tectorins, calbindin D28K and bone/dentin matrix proteins, in order to identify additional compensatory events.

An antibody against the sulfated chain of KSPG (keratin sulfate proteoglycan) showed intense fluorescent signals in the otoconial membrane (OM) and the luminal extracellular matrix (ECM) of all vestibular epithelia (Figures 4A, 4B) in both wt and null tissues. Staining in wt otoconia was moderate and mostly on the outer rim of the crystals (“O” in Figures 4A, 4B), and staining in null otoconia was similar and on the outer surface. This KSPG staining on the outer surface of the giant otoconia may account for the appearance of one matrix layer embracing all the aggregated crystallites in Oc90 null mice (Zhao et al. 2007). There was no significant difference in KSPG staining intensity in the OM or ECM between the two genotypes.

In contrast, none of the antibodies for various moieties of HSPG, including the heparin/heparin sulfate side chain and the core protein, detected any signal in the crystals or OM in Oc90 wt or null vestibules (Figures 4C, 4D). There was faint staining on the luminal surface of the epithelia. The antibodies detected HSPG in cartilage (labeled as “C”), consistent with the literature that HSPG is a major proteoglycan in cartilage and bone. Nerve fibers (“N”) were also stained. D M B proteoglycan assay, which detects the sulfated glycosaminoglycan chains of all proteoglycans, showed no significant difference in the total proteoglycan content in the epithelia (including attached matrices) of Oc90 wt and null mice (Figure 4E). Since KSPG was the predominant proteoglycan in the epithelial and matrix tissues of the vestibule, the total KSPG amount was therefore estimated to be similar between the two genotypes, confirming the findings from fluorescent immunostaining.

Calbindin D28K, an otoconial component in some but not all species (Usami et al. 1995;Karita et al. 1999;Balsamo et al. 2000;Piscopo et al. 2004), was not detected in wt or Oc90 null murine otoconia either by immunostaining or Western blotting, while strong signals were seen in hair cells, ganglia, nerve fibers, and cartilage (date not shown). The present immunostaining results agree with previous reports that the protein is localized within afferent neuronal components in sensory organs, where it may regulate Ca^{2+} levels for optimal neurotransmission in the primate, other mammalian and avian auditory and vestibular systems (Usami et al. 1995;Buckiova and Syka 2009).

Both α- and β-tectorins were abundant in the ECM and OM (Figures 5A–5D) of Oc90 wt and null vestibules, but absent in the crystals except for faintly stained crystal surfaces with the α-tectorin antibody in both genotypes (“O” in Figures 5C, 5D). This observation suggests that the level of α-tectorin in otoconia is low, if any, and that the reduced otoconia layer in α-tectorin null mice (Legan et al. 2000) may have arisen from a defect in the OM (i.e., reduced or even missing OM). In any case, our data indicate that Oc90 and α-tectorin (or β-tectorin) probably do not co-exist as an interacting complex in the organic matrix of wt otoconia, as the deposition (or lack of it) of the latter proteins is unaltered in Oc90 null crystals. The abundant presence of *α*-tectorin and β-tectorin in the OM and their absence in the crystals suggest that the OM, rather than otoconia crystals, is homologous to the tectorial membrane (TM) in their components and ultrastructures. *α*-tectorin is the major non-collagenous protein of the TM (Killick et al. 1995;Legan et al. 1997;Legan et al. 2000), and has three full and two partial vWF domains, a Zona pellucida (ZP) domain and a nidogen domain. Other components of the TM include β-tectorin, otogelin, and possibly Oc90, which

are all present in the OM (Cohen-Salmon et al. 1997;Killick et al. 1995;Zhao et al. 2007). However, functionally the crystals are likely the counterpart of the TM since their absence leads to absent VsEPs as in the otopetrin 1 and Nox3 mutants (Jones et al. 1999;Jones et al. 2004;Zhao et al. 2007).

The zebrafish otolith protein, Starmaker, leads to abnormal otolith growth when knocked down (Sollner et al. 2003;Zhao et al. 2007). Although there is no mammalian ortholog of Starmaker, based on the amino acid composition and functions, dentin sialophosphoprotein (DSPP) is probably the closest functional analog in mammals. DSPP gives rise to two mature products, dentin sialoprotein (DSP) and dentin phosphoprotein (DPP), and both are present in the calcified matrix of teeth and bone. However, DSP was not detected in wt or null otoconia (data not shown). The protein was detected in inner ear cartilage but not in vestibular epithelia. The absence of DSP in otoconia and vestibular epithelia was also confirmed by Western blotting (data not shown). Another major dentin/bone matrix protein, dentin matrix protein 1 (DMP1), showed no staining in wt otoconia and faint staining in Oc90 null crystals (data not shown). Semi-quantitative Western blotting of wt otoconia extracts showed a weak band in the expected size range (~55 kD) but did not detect any increase of DMP1 in Oc90 null otoconia (data not shown), therefore the observed slight increase in immunostaining is likely insignificant. Both DMP1 and DSP have high levels of carbohydrate and sialic acid, resembling other sialoproteins such as osteopontin, which is present in otoconia. These data are summarized in Table 2.

Either Oc90 or Sc1 can facilitate calcification

NIH/3T3 cells stably transfected with Oc90 or Sc1 augmented ECM calcification after 5 days of induction with 0.5 mM Ca^{2+} and 2mM Pi (Figure 6). The Ca^{2+} concentration here is much lower than that used in osteoblast calcification studies (a minimum of 2 mM for the latter); the Pi concentration is slightly lower too (a minimum of 2.5 mM) (Murshed et al. 2005). In the figure, inorganic calcium deposits were visualized with ARS staining, and proteins by fluorescent immunostaining. Percentages of cells with ECM calcification over total cells were obtained. In order to rule out the effect of cell density on calcification, all cells were grown to confluence when calcification was examined. No calcification was seen in untransfected or transfected cells cultured in standard media without additional supplements of Ca^{2+} and Pi (Figure 6A). Under identical culture and inducing conditions, ratios of cells with ECM calcification were similar between untransfected cells and cells transfected with empty vectors. Among cells stably transfected with Oc90 (Figure 6D), an average of 4.8±0.8% cells had matrix calcification under 0.5 mM Ca^{2+} and 2mM Pi, as compared to 1.2±0.2% for those transfected with the empty vector (Figure 6B) ($p<0.001$, n=3 experiments×3~4 survey fields in each). Among cells stably transfected with Sc1 (Figure 6C), an average of 3.8±0.7% cells had matrix calcification ($p<0.001$ vs. empty vector, n=3 experiments×3~4 survey fields in each). Due to the large number of confluent cells in each view field, the percentages of calcification nodules become small; therefore, averaged counts of calcification nodules versus total cells in each survey field are presented in Supplemental Table S1. The effect of Oc90 on calcification was significantly stronger than that of Sc1 ($p<0.001$). Besides being matrix components (Figure 6C, D, F), both Oc90 and Sc1 have been detected in the endolymph and cell culture media, respectively (Verpy et al. 1999;Mendis et al. 1996b)(Lundberg, unpublished observation), and could exert an inductive effect on the cells and/or matrix to increase ECM calcification as well.

Although the cell culture condition is likely different from that *in vivo*, the findings here can suggest, beyond the *in vivo* evidence, the likelihood that Oc90 and Sc1 can facilitate calcification. *In vivo*, measurements of endolymph [Ca^{2+}] are extremely low, at ~20–50 μM, with some reporting higher in the vestibule (above 200 μM) especially during developmental stages (Wood et al. 2004;Marcus and Wangemann 2009;Wangemann et al.

2007;Salt et al. 1989). As a result of nearby PMCA2 and other Ca^{2+} pumps, the micro-environmental [Ca^{2+}] near and within the extra-cellular matrix could be very high, which remains unknown.

Homology modeling of Oc90 and Sc1

The 50% reduction of averaged otoconia mass in Oc90 null mice (Zhao et al. 2007) and the compensatory increase in Sc1 deposition in Oc90 null otoconia show that Oc90 and Sc1 can both serve as the otoconial matrix and promote calcification. The latter is also suggested by the *in vitro* calcification study. We hypothesized, therefore, that the two proteins may share some features that are important for inorganic calcium phosphate (or carbonate) to deposit and grow. The two proteins have no significant sequence similarity, but: (1) Both are extremely acidic due to the large numbers of Glu and Asp residues, with 28x Glu and 39x Asp out of 468 aa. in mature Oc90, and 52x Glu and 87x Asp out of 634 aa. in mature Sc1 (supplemental Table S2); these residues confer a high affinity for apatite/hydroxyapatite (Bolander et al. 1988;Fujisawa et al. 1996), and possibly for calcite. (2) Both are rich in Cys (34x Cys in mature Oc90; 14x Cys in mature Sc1 and all in its Sparc-like domain, see supplemental Table S2 and S6), and are predicted to form intermolecular disulfide bridges to oligomerize and form a rigid and stable framework to ensure optimal interface with the inorganic crystals. (3) Both can potentially bind collagen (Brekken and Sage 2001;Hambrock et al. 2003;Sweetwyne et al. 2004;Zhao et al. 2007) and form a complex structural network for ordered mineral deposition. (4) Both have Ca^{2+}-binding domains, such as EF-hand motifs, which can also bind calcite and apatite. The C- and N- terminal regions of Oc90 and Sc1, respectively, are potential flexible Ca^{2+}-binding regions. (5) Both have α-helices (Figures 7 and 8) that may be important for interacting with Ca^{2+}, inorganic crystals or matrix proteins. These structural features of Oc90 and Sc1/Sparc are highly conserved throughout evolution as described below and presented in supplemental Table S3–S7.

To identify additional common features, we used homology modeling and subsequent molecular dynamics simulation to obtain the tertiary structures of these proteins (Figures 7 and 8). The structural stability of the homology models was assessed by calculating the root mean square deviation (RMSD) of the backbone atoms along the trajectory. Since the C-terminal tails (the last 21 residues) in both Oc90 domains have flexible structures, they were left out from the analysis. Nevertheless, the RMSD of residues 1–102 shows that during MD simulation the structures quickly reached equilibrium and then they are fluctuated around an average structure (Figures 7B, 7C). For both Oc90 domains, over the entire simulation's time-averaged structures were constructed. The RMSD of the two overlaid time-averaged structures is 1.626 Å (Figure 7D). The seemingly high RMSD reflects the structural differences in the C-terminal tail of the two models. Furthermore, the final structures show high structural similarity with experimental PLA2 structures. For example, RMSD of the overlaid structure of Pla2l-D1 and a human PLA2 (PDB entry 1KQU) is 1.517 Å (Figure 7E). It should be noted that for this comparison the structure of the selected human PLA2 was not part of the model building. Therefore, the high 3D similarity between the predicted and experimental structures reflects the high quality of the homology model.

For Sc1 modeling, the homology builder only identified structures from the PDB that have similarities in its Sparc-like domain (Figure 8A). Subsequently, a hybrid homology model was built from 10 templates for residues 489 to 650 (Figure 8B). Backbone RMSD analysis of the MD trajectory of 65 ns simulation shows that the structure of Sc1 reaches equilibrium at 8 ns and from that point on it fluctuates around and average structure (Figure 8C). The time-averaged structure, which was obtained over the entire simulation, was overlaid with the X-ray structure of human SPARC (PDB id 1SRA) (Hohenester et al. 1996) (Figure 8B). The low RMSD value (1.023 Å) indicates high 3D structural similarity between the two

proteins, therefore, the hybrid homology model most likely represent the Ca^{2+}- and collagen-binding domain of Sc1 (see below).

Murine Sc1 (418–650) shares 87% sequence similarity (counting conservative variations) to murine Sparc (70–302) (Swiss-Prot id P07214) (Figure 8A). This region contains an EF-hand motif (608–643) and a second Ca^{2+}-binding domain (621–632) that also bind several types of collagen (Hambrock et al. 2003;Hohenester et al. 1996;Maurer et al. 1995;Soderling et al. 1997). Sparc itself is an extremely conserved protein throughout evolution, with zebrafish, xenopus, chicken, mouse and human orthologs sharing >90% aa. homology (supplemental Table S7). While the N-terminal half of Sc1 is more variable, the Sparc-like domain of Sc1 (419–650) is extremely conserved, with the above species sharing >90% aa. homology as well (supplemental Table S5). Similarly, the Pla2l domains of Oc90 (Oc22 in xenopus) are highly conserved among zebrafish, xenopus, chicken, mouse and human (supplemental Table S3), especially so among the latter 3 species which share 86% and 80% aa. homology in Pla2l-D1 and -D2, respectively (supplemental Table S4).

Discussion

In this study, we have discovered a vast increase in Sc1 incorporation in murine otoconia in the absence of Oc90, and have demonstrated a possible role for Sc1 in biomineralization, which is previously unknown. After examining additional candidates, we conclude that the observed increase is specific to Sc1 and, to a much less degree, Sparc. Protein structural analysis and modeling suggest structural requirements that renders a protein high affinity for calcite (in otoconia), and perhaps also apatite/hydroxyapatite (in bone and teeth), crystals.

Sc1 was recently identified in dissected wt murine otoconia by mass spectrometry (Thalmann et al. 2006); here we have further validated this finding by *in vivo* studies. However, Sc1 knockout mice have a normal phenotype (McKinnon et al. 2000) and show no significant vestibular dysfunction (S. Funk and H. Sage communication through Thalmann et al., 2006), indicating that the protein is dispensable or a functionally redundant protein has compensated for its loss. It is unclear whether these mice have minor otoconia defects, which would not manifest any obvious imbalance behavior. In wt mice, Sc1 is widely expressed in the brain and can be detected in many types of neurons (Johnston et al. 1990;Mendis and Brown 1994;McKinnon and Margolskee 1996;Lively et al. 2007), whereas Sparc (aka BM-40 and osteonectin) is generally present in tissues undergoing remodeling including skeletal formation and maintenance, angiogenesis, and injury repair (Bolander et al. 1988;Hohenester et al. 1997;Sage and Vernon 1994). Both Sc1 and Sparc regulate cell-cell and cell-matrix interactions by binding to structural matrix proteins, and inhibit cell adhesion by disrupting focal adhesions. So far, studies on Sc1 have been focused on the nervous system and tumorigenesis.

Sparc has recently been identified in fish otoliths (Kang et al. 2008). The mechanism through which Sparc regulates crystal growth may be similar to OMP since Sparc, as well as Sc1, has an extracellular Ca^{2+}-binding domain (EC) which also has affinity for several collagen types (Hambrock et al. 2003;Hohenester et al. 1996;Maurer et al. 1995;Soderling et al. 1997). Thus, either Sparc or OMP can bind otolin-1, a member of the collagen X family, in otoliths. Conceivably, Sparc and Sc1 can partially compensate for the loss of Oc90 due to their structural similarities as noted in the Result section. Oc90 may have a higher affinity for calcite than Sc1 and Sparc, which makes it a preferred molecule in normal otoconia assembly in wt mice. But when Oc90 is absent, there may be some feedback which increases the recruitment of Sc1 and Sparc to partially make up for their lower affinity for calcite, thus promote an alternative method of biomineralization. Although such an increase in protein deposition does not fully reverse the effects of Oc90 deletion, the remnant otoconia in Oc90

null mice are able to render significant functional compensation, as demonstrated by the mild and less frequent occurrence of imbalance behaviors and greater trained improvement of performance compared to the otoconia-absent mutants (Zhao et al. 2008b). Therefore, it may be argued that, in various human otoconia deficiencies, even a low level of rescue will help a great deal in preserving and recovering balance functions.

The interactions of bone matrix proteins with hydroxyapatite (or apatite) include two modes: those that directly bind the inorganic crystals and those that interact with crystal-binding proteins. In either case, charged residues in specific positions, particularly Glu and Asp, serve as crystal nucleation centers. For example, Glu and Asp are found to be required for a protein to nucleate apatite crystals *in vitro* (He et al. 2003;Murphy et al. 2007;Boanini et al. 2006), which may implicate the principle that electrostatic energy plays a dominant role in guiding the adsorption of selective proteins (Shen et al. 2008). In the second mode, matrix proteins, such as DMP1 and osteopontin, bind to type I collagen and regulate crystal growth (He et al. 2005;Ito et al. 2004). In such cases, positions of charged amino acids along the three alpha-chain axes of type I collagen, also including Glu and Asp, as well as Lys, Arg, hydroxylysine and His, specify unique sites of potential apatite nucleation centers following binding of calcium and phosphate ions (Landis and Silver 2009).

Oc90, Sc1 and Sparc all are rich in acidic residues. Furthermore, our data demonstrate that Cys may also be critical for calcite (possibly also apatite and hydroxyapatite) crystal-binding. Western blotting (Figure 2A) suggests that the enriched Cys likely form intermolecular disulfide bonds and cause the protein to dimerize (or maybe even oligomerize) to stabilize the inorganic crystals. A reminiscent case is that DMP1 in solution was found to oligomerize and temporarily stabilize the newly formed calcium phosphate nanoparticle precursors by sequestering them and preventing their further aggregation and precipitation (He et al. 2005), despite that mature DMP1 only has one Cys residue. Alternatively, the Cys-rich proteins may form intra-molecular disulfide bridges, which has been demonstrated by Chun et al (Chun et al. 2006). This feature likely renders the molecule a rigid and stable conformation ideal to serve as a lattice for crystal deposition and/or growth. However, some important calcified matrix proteins, such as osteopontin, do not have Cys.

Intriguingly, the other bone/dentin matrix proteins are either absent in otoconia or dispensable for calcite crystal formation. For example, deletion of osteopontin leads to altered crystal sizes and increased mineral content in bone (Boskey et al. 1993;Hunter et al. 1994;Shapses et al. 2003), but does not affect otoconia formation or balance function (Zhao et al. 2008b). The function of osteopontin in bone is reminiscent of that of Oc90 in otoconia. Fetuin-A is unlikely to play a critical role in crystal formation because (1) the protein has a similar level in Oc90 wt and null otoconia (Zhao et al. 2007), (2) fetuin-A null mice have normal bone calcification under normal dietary conditions (Jahnen-Dechent et al. 1997) despite the abundant accumulation of fetuin-A in wt bone, and (3) the null mice have no apparent imbalance behaviors (Jahnen-Dechent communication in Thalmann et al., 2006). Despite the critical roles of DSP and DMP1 in apatite crystal seeding and growth in teeth and bone, the former is not detectable in wt or Oc90 null crystals, and the latter is only present at a very low level. Like osteopontin (aka Spp1), these two also belong to the family of glycophosphoproteins that are called small integrin-binding ligand N-linked glycoproteins (SIBLINGs) (Fisher and Fedarko 2003;Fisher et al. 2001;Bellahcene et al. 2008), which are a sub-family of the SCPPs (Secretory Calcium-binding Phospho-Proteins), while Sc1 and Sparc belong to the larger SCPP family (Kawasaki and Weiss 2008). These polyanionic SIBLING proteins also play key roles in the mineralization of bone and dentin (Toyosawa et al. 2001;MacDougall et al. 1998).

Indeed, many of the non-collagenous proteins regulating ECM mineralization belong to the SCPP family. Interestingly, different sub-groups of proteins in the SCPP family do not share amino acid sequence similarity; in fact, most of these proteins (e.g. Spp1) are highly divergent from teleosts to mammals in the amino acid sequences of the orthologs. Oc90 does not belong to the SCPP family and does not have sequence similarity with Sc1/Sparc either. Yet, these proteins can all efficiently facilitate biomineralization. Therefore, the noted features must be both crucial and sufficient for such a function; or they may be functioning in different aspects of the processes that lead to the same outcome. For example, some may interact with the bone/dentin scaffold protein collagen I to augment the strength and/or expansion of the organic matrix network; some others may directly bind the inorganic crystals.

The role of proteoglycans in the initiation and stabilization of calcite biomineral form remains untested. A proteoglycan consists of a core protein and long sugar chains called glycosaminoglycans (GAGs). Proteoglycans are components of the cell membrane, intracellular granules and the extracellular matrix, and are involved in cell adhesion, migration, proliferation and differentiation. Proteoglycans have been found to be involved in the calcification process of fish otoliths (Borelli et al. 2003;Borelli et al. 2001), and KSPG has been reported in chicken and chinchilla otoconia (Fermin et al. 1990;Swartz and Santi 1997). These molecules are critical players of bone/teeth biomineralization, with HSPG and CSPG as the main ones in bone and cartilage. At the onset of dentin formation, it is speculated that the protein cores may organize the collagen network for receipt of phosphoproteins and phospholipids; the rigid, spatially oriented GAG chains bind Ca^{2+} and may participate directly in mineral initiation (Yamakoshi et al. 2005;Embery et al. 2001). Deletion or depletion of major proteoglycans leads to reduced capacity of bone and cartilage formation and various calcification deficiencies (Funderburgh 2000;Young et al. 2002;Hassell et al. 2002;Xu et al. 1998;Viviano et al. 2005).

Although the focus of the present work is otoconia constituents, we would like to point out that altered expression and/or function of regulatory proteins is possible in the absence of Oc90. Such otoconia-regulatory proteins include Otopetrin 1(Hurle et al. 2003;Hughes et al. 2007;Sollner et al. 2004), NAD(P)H oxidase 3 (Nox3) (Paffenholz et al. 2004;Banfi et al. 2004), and Nox organizer 1 (Noxo1) (Kiss et al. 2006), whose mutant forms all lead to absent otoconia formation. The Nox activator Noxa1 may also optimize otoconia formation due to its presence in embryonic inner ear (Kiss et al. 2006).

Conclusion

We have detected a drastic increase of Sc1 deposition in Oc90 null otoconia and have shown that this up-regulation is specific to Sc1 after screening a comprehensive list of candidate proteins including proteoglycans, tectorins, calbindin and bone/dentin matrix proteins. Furthermore, we have shown that Oc90 and Sc1 can indeed facilitate ECM calcification in NIH/3T3 cells, and have identified common structural features of Oc90 and Sc1 proteins that may be critical to enable a protein to serve as the backbone for efficient biomineralization in multiple organs (particularly otoconia and bone). Such information yields important insight toward understanding how these critical players influence otoconia morphogenesis and possibly systemic calcification, and will serve as the foundation for future regenerative purposes.

Experimental Procedures

Mice

Oc90 null mice were previously generated and the absence of Oc90 protein in the null mutants was established (Zhao et al. 2007). The mice were backcrossed to C57BL/6J (as C57). Unless otherwise indicated, the reported results were all obtained from homozygous mutants. All animal procedures were approved by the Institutional Animal Care and Use Committee at the Boys Town National Research Hospital in accordance with federal and international guidelines.

Histology

Inner ears were dissected, fixed in 4% paraformaldehyde, dehydrated in 30% sucrose, embedded in OCT under −20°C (or −80°C) and sectioned at 9 μm. Inner ears at postnatal stages were partially decalcified in 0.25 M EDTA (pH7.4) for 2 hours to overnight, depending on the age of the animals.

Fluorescent immunostaining

Detailed information on the suppliers and working dilutions of antibodies are provided in Table 1. Antibodies for tectorins were kindly provided by Dr. Guy P. Richardson at the University of Sussex, UK (Knipper et al. 2001) and were used at 200x dilution.

Frozen vestibular sections were blocked in blocking solution containing 5% goat serum (or 5% BSA depending on the primary antibodies used) and 0.2% Triton-X-100 in PBS at room temperature for 30 minutes. Primary antibodies were added at optimized dilutions and incubated at 4°C overnight. After 3 washes in 1×PBS, an Alexa-488 or 568 (Molecular Probes, Carlsbad, CA, USA) conjugated secondary antibodies were added at a dilution of 1:600, together with DAPI (1:10000), and incubated at room temperature for 2 hours in the dark. Non-immunized sera instead of primary antibodies were used in some sections as negative controls. Slides were mounted in Fluoromount-G and signals were viewed using a Zeiss LSM 510 confocal microscope. Some observations were made using a Zeiss AxioImager.A1 fluorescent microscope.

To minimize experiment-introduced variations, all tissue sections in comparison were done under strictly the same conditions (e.g. identical immunostaining procedures, identical confocal scanning parameters and the same number of fluorescent exposures). Cross sections that cover both the striola and peri-macular region were used to take into consideration possible intensity difference caused by the position and orientation of cells and sections. 2–3 sections (e.g. every 10^{th} section) from each of 3 mice were analyzed for each genotype/age group. Results from these analyses were confirmed by semi-quantitative Western blotting.

Assaying for protein concentrations and total protein content

Protein concentrations were measured using a Micro-BCA (bicinchoninic acid) Protein Assay Kit (Pierce, Rockford, IL, USA) following the manufacturer's protocol. Briefly, 50 μl of each diluted BSA standards and protein samples were added into microplate wells; 50 μl of freshly prepared working reagent (A:B:C @ 25:24:1) was added into each well and mixed gently. Duplicates to triplicates were done on each standard or test sample. The reaction was incubated at 37°C for 2 hours with rocking, and the absorbance was measured at 562 nm on a Quant MQX200 plate reader (Bio-Tek Instruments, Inc., Winooski, VT, USA). Sample protein concentrations were calculated according to standard curves.

Semi-quantitative Western blotting

Proteins from dissected and pooled otoconia and epithelia of the utricule/saccule and cochlea were extracted in lysis buffer containing 40 mM Tris, 4% CHAPS, 8 M urea, 10 mg/ml DTT (dithiothreitol) and 0.15 M EDTA. EDTA, buffer and salts in otoconia were removed by passing through Centricon columns (Millipore, Billerica, MA, USA) after 20-fold dilution. Protein concentrations were determined using a Micro-BCA protein assay kit as described above. An aliquot of each sample containing an equal amount of total protein was mixed with 2X sample loading buffer (0.13 M Tris-HCl, 20% glycerol, 46 mg/ml SDS, 0.2 mg/ml bromophenol blue, 20 mg/ml DTT), boiled for 5 minutes, loaded onto a 4–20% gradient Tris-HEPES-SDS gel (Pierce), electrophoresed at 150 V in Tris-HEPES-SDS running buffer (100 mM Tris, 100 mM HEPES, 3mM SDS) for 45min, and transferred to a PVDF membrane (Millipore) at 100V for 1 hour. The blot was washed once with TBST buffer (50 mM Tris, 150 mM NaCl, 0.1% Tween-20) and treated with 1% blocking buffer (Roche Applied Science, Indianapolis, IN, USA) for 2 hours at room temperature. The membrane was incubated with a primary antibody at an optimized dilution (1:500) overnight at 4°C followed by 3 washes in TBST buffer, and incubated with a corresponding peroxidase-conjugated secondary antibody (Sigma, St. Louis., MO, USA) at 1:10,000 dilution for another 3 hours. After 3 washes, detection solution was added for 1 minute, and the blot was exposed to a Kodak X-ray film and imaged using the Canoscan 8400F imaging station. Some membranes were stripped in Restore Western Blot Stripping Buffer (Pierce) and re-used for detection with several antibodies (separately) against different proteins.

Real-time quantitative RT-PCR (qPCR)

Total RNA was isolated using Trizol (Invitrogen, Carlsbad, CA, USA). First-strand cDNA was synthesized from 1 μg total RNA with random hexamer primers using the SuperScript III First-Strand Synthesis System (Invitrogen). TaqMan gene expression assays were purchased from Applied Biosystems (Foster City, CA, USA) and real-time quantitative PCR reactions (40 cycles) were performed with an ABI Prism 7900HT Sequence Detection System (Applied Biosystems) according to the manufacturer's protocols. Mouse β-actin (*Actb*) gene was used as an endogenous control for normalization. Reactions were performed in at least triplicates. The probe sequences were: *Sc1* - AGCCACCTCTCCGCAGATCTAGCCA (ABI i.d. Mm00447780_m1); *Sparc* - AGAAGCAGAAGCTGCGTGTGAAGAA (Mm01295757_g1); and β-*actin* – TTACTGAGCTGCGTTTTACACCCTT (Mm00607939_s1).

Dimethyl-methylene blue (DMB) proteoglycan assay

Proteoglycans were measured using the colorimetric method of Farndale, Sayers & Barret (Farndale et al. 1982) and Farndale, Buttle & Barrett (Farndale et al. 1986) with some modifications. Pooled tissues were blotted dry, weighed and digested in 0.5 ml papain (16.3 U/ml) in 20 mm disodiumhydrogen-orthophosphate dihydrate, 1 mm EDTA and 2 mm DTT (Sigma). After incubation at 65°C for 2 h, 50 ul of each digest was diluted 1:8 with the digestion buffer, and duplicate aliquots (10 μ1) of the diluted digest and of standard whale chondroitin sulphate (Sigma) were added to a microtiter plate. DMB was prepared by dissolving 16 mg of the dye (Sigma), 3.04 g glycine and 2.37 g NaCl in deionized water (final volume 1 L, pH 3.0). DMB (200 μl) was added to each well and the absorbance at 525 nm (reference wavelength 690 nm) was read immediately using a Quant MQX200 plate reader (Bio-Tek Instruments). The change in absorbance was calculated from the mean absorbance of six blank wells in which only buffer and dye were added. The plate reader was interfaced with a computer to facilitate calculation of the concentration of proteoglycans in the samples from the standard curve. All reactions were performed in duplicates, and 4–6 pooled samples, each consisted of 2 mice, were analyzed.

Construction of expression vectors

Full-length *Oc90* (stop codon omitted) and *Sc1* transcripts were amplified by RT-PCR of postnatal mouse inner ear tissues and unidirectionally cloned into pTracer-EF/V5-His(C) (pOc90) and pcDNA3.1 (pSc1). The RT-PCR primers were 5'-ggaattcATGATTATGCTGCTCATGGTCGGT-3' and 5'-gctcgagTTTCCCACCGAGGGGTCTGGCCC-3' for *Oc90*, and 5'-aacaagcttATGAAGGCTGTGCTTCTCCTC-3' and 5'-acactcgagTCAAAAGAGGAGGTTTTCATC -3' for *Sc1*. Nucleotides in lower cases were non-endogenous sequences to create restriction sites for cloning, and restriction enzymes used were EcoR I and Xho I for *Oc90*, and HindIII and Xho I for *Sc1*. Constructs were confirmed by DNA sequencing and correct protein expression was confirmed by Western blotting.

Cell culture and stable transfection

NIH/3T3 cells were cultured in DMEM containing 4.5 g/L glucose, 100 U/ml penicillin, 4 mM L-glutamine and 10% fetal bovine serum. Conventional culture condition was used at 37°C in a humidified incubator supplemented with 5% CO_2. The cells were transfected with pOc90, pSc1, pcDNA3.1 or pTracer using FuGene (Roche Applied Science, Indianapolis, IN). Stably transfected clones were selected over a two-week period using 400 ug/ml Zeocin for pOc90, or 800 ug/ml G418 for pSc1. Selected clones were then expanded and analyzed for calcification potential as described below.

Induction of calcification

To induce ECM (extra-cellular matrix) mineralization, stable NIH/3T3 clones expressing pOc90, pcDNA3.1-Sc1, pcDNA3.1 or pTracer were treated with 0.5 mM Ca^{2+} ($CaCl_2$) and 2mM Pi (Na_2HPO_4) in growth media to provide a source of inorganic components for mineralization. Phosphate, instead of carbonate, was used so as not to alter the optimal pH and CO_2 content. After 5 days of induction, cells were fixed with 4% PFA, and stained with Alizarin Red S (ARS) (Chemicon, Billerica, MA) and/or antibodies. The effects of various Ca^{2+} and Pi concentrations were tested to determine the optimal condition at which the effects of Oc90 or Sc1 were best differentiated from empty vectors. Preliminary experiments showed that Sc1 slowed cell proliferation, as reported by others (Esposito et al. 2007;Claeskens et al. 2000). If Sc1 cells were plated at a number 1.5 times that for other cells, on the 6^{th} day when calcification was analyzed, the cell density would be similar among different cell transfectants. The supplemental Ca^{2+} and Pi reduced the proliferation rate of all cells, whether they were transfected or not. For the reported results, 3×10^4 Sc1 cells and 2×10^4 other cells were plated in each well of the 24-well plate. Calcification nodules and total cells were photographed and counted for each 20x view field under an inverted microscope (approximately 1.2 mm^2); averaged ratios of nodules/total cells were compared among transfectants and the empty vector using Student's t-test.

Homology modeling of the structures of Oc90 and Sc1

The three-dimensional (3D) structure for neither OC90 nor Sc1 is available, therefore, homology modeling was used to predict it. Homology models were built using the YASARA molecular modeling package (Krieger et al. 2002). For all modeling the hm_build.mcr macro of the YASARA package was used with the built-in parameters except the maximum oligomerization state was set to one.

Oc90 modeling—Oc90 contains two phospholipase A2-like (Pla2l) domains at residues 75–197 and 314–436 (bolded and underlined in Figure 7A). When the whole sequence of OC90 was submitted to homology modeling, YASARA only identified the first Pla2l

domain, therefore, the protein was fragmented into three separate sequences to be modeled separately: Pla2l-D1 (residues 75–197), loop region (residues 198–313, which connects the two Pla2l domains) and Pla2l-D2 (residues 314–436). For the loop region YASARA did not identified any homology model. For Pla2l-D1, from the protein data bank (PDB) 10 template structures (PDB i.d.: 1BPQ, 1G4I, 2ZP3, 1HN4, 1VL9, 1OW3, 2B00, 2BAX, 3ELO and 3CXI) were used to build a hybrid model. Since this model had worst Z-score (−0.912) (Hooft et al. 1996) than that of the Pla2 analog with 1BPQ PDB entry (−0.848), the latter was selected to build the final model. For Pla2-D2, from the protein data bank 11 template structures (PDB i.d.: 1S6B, 1YXH, 2ZP3, 3GCI, 1VL9, 1G4I, 4BP2, 1MF4, 3ELO, 3CXI) were used to build a hybrid model with overall Z-score of −0.722. Both models were subjected to further refinement using the md_refine.mcr macro of YASARA and finally the refined models were subjected to 5.5 ns constant temperature and pressure (NPT) molecular dynamics (MD) simulations using the md_run.mcr macro of YASARA. Simulation parameters were kept at the values defined by the macro. The structure of the protein was simulated in a 8 × 6 × 5 nm rectangular box with periodic boundaries. The box containing the protein was filled with 1834 water molecules. The simulation used the AMBER03force field.

Sc1 modeling—The whole sequence of Sc1 (Swiss-Prot id P70663) was submitted to modeling. The hm_build.mcr macro of YASARA identified 10 templates (PDB i.d.: 1BMO, 1NUB, 2V53, 1SRA, 3HH2, 3B4V, 2ARP, 1LR7, 2P6A and 2KCX) from the protein data bank to build a hybrid model with a Z-score of 0.386. The hybrid model was subjected to further refinement using the md_refine.mcr macro of YASARA and finally the refined model was subjected to 65 ns NPT molecular dynamics (MD) simulations using the md_run.mcr macro of YASARA. Simulation parameters were kept at the values defined by the macro. The structure of the protein was simulated in a 7.6 × 6.5 × 6.4 nm rectangular box with periodic boundaries. The *N*-acetyl and *N*-methyl amide protecting groups were added to the N and C-terminus, respectively, in order to preserve the electronic structure of the backbone from the whole protein. The box containing the protein was filled with 2707 water molecules. The simulation used the AMBER03force field.

Supplementary Material

Refer to Web version on PubMed Central for supplementary material.

Acknowledgments

We thank Dr. Guy P. Richardson for the generous gifts of tectorin antibodies, and Drs. Helene Sage and Peter J. McKinnon for providing partial-length Sc1 expression constructs. The work was supported by a grant from the National Institute on Deafness and Other Communication Disorders (RO1 DC008603 and DC008603-S1 to Y.W.L.) and from the National Center for Research Resources (P20 RR016469 to S.L.).

Reference List

Balsamo G, Avallone B, Del GF, Trapani S, Marmo F. Calcification processes in the chick otoconia and calcium binding proteins: patterns of tetracycline incorporation and calbindin-D28K distribution. Hear Res. 2000; 148:1–8. [PubMed: 10978820]

Banfi B, Malgrange B, Knisz J, Steger K, Dubois-Dauphin M, Krause KH. NOX3, a superoxide-generating NADPH oxidase of the inner ear. J Biol Chem. 2004; 279:46065–46072. [PubMed: 15326186]

Bellahcene A, Castronovo V, Ogbureke KU, Fisher LW, Fedarko NS. Small integrin-binding ligand N-linked glycoproteins (SIBLINGs): multifunctional proteins in cancer. Nat Rev Cancer. 2008; 8:212–226. [PubMed: 18292776]

Boanini E, Torricelli P, Gazzano M, Giardino R, Bigi A. Nanocomposites of hydroxyapatite with aspartic acid and glutamic acid and their interaction with osteoblast-like cells. Biomaterials. 2006; 27:4428–4433. [PubMed: 16682075]

Bolander ME, Young MF, Fisher LW, Yamada Y, Termine JD. Osteonectin cDNA sequence reveals potential binding regions for calcium and hydroxyapatite and shows homologies with both a basement membrane protein (SPARC) and a serine proteinase inhibitor (ovomucoid). Proc Natl Acad Sci U S A. 1988; 85:2919–2923. [PubMed: 2834720]

Borelli G, Mayer-Gostan N, De PH, Boeuf G, Payan P. Biochemical relationships between endolymph and otolith matrix in the trout (Oncorhynchus mykiss) and turbot (Psetta maxima). Calcif Tissue Int. 2001; 69:356–364. [PubMed: 11800233]

Borelli G, Mayer-Gostan N, Merle PL, De PH, Boeuf G, Allemand D, Payan P. Composition of biomineral organic matrices with special emphasis on turbot (Psetta maxima) otolith and endolymph. Calcif Tissue Int. 2003; 72:717–725. [PubMed: 14563001]

Boskey AL, Maresca M, Ullrich W, Doty SB, Butler WT, Prince CW. Osteopontin-hydroxyapatite interactions in vitro: inhibition of hydroxyapatite formation and growth in a gelatin-gel. Bone Miner. 1993; 22:147–159. [PubMed: 8251766]

Brekken RA, Sage EH. SPARC, a matricellular protein: at the crossroads of cell-matrix communication. Matrix Biol. 2001; 19:816–827. [PubMed: 11223341]

Buckiova D, Syka J. Calbindin and S100 protein expression in the developing inner ear in mice. J Comp Neurol. 2009; 513:469–482. [PubMed: 19226521]

Chun YH, Yamakoshi Y, Kim JW, Iwata T, Hu JC, Simmer JP. Porcine SPARC: isolation from dentin, cDNA sequence, and computer model. Eur J Oral Sci. 2006; 114 Suppl 1:78–85. [PubMed: 16674666]

Claeskens A, Ongenae N, Neefs JM, Cheyns P, Kaijen P, Cools M, Kutoh E. Hevin is down-regulated in many cancers and is a negative regulator of cell growth and proliferation. Br J Cancer. 2000; 82:1123–1130. [PubMed: 10735494]

Cohen-Salmon M, El-Amraoui A, Leibovici M, Petit C. Otogelin: a glycoprotein specific to the acellular membranes of the inner ear. Proc Natl Acad Sci U S A. 1997; 94:14450–14455. [PubMed: 9405633]

Davis JG, Oberholtzer JC, Burns FR, Greene MI. Molecular cloning and characterization of an inner ear-specific structural protein. Science. 1995; 267:1031–1034. [PubMed: 7863331]

Embery G, Hall R, Waddington R, Septier D, Goldberg M. Proteoglycans in dentinogenesis. Crit Rev Oral Biol Med. 2001; 12:331–349. [PubMed: 11603505]

Esposito I, Kayed H, Keleg S, Giese T, Sage EH, Schirmacher P, Friess H, Kleeff J. Tumor-suppressor function of SPARC-like protein 1/Hevin in pancreatic cancer. Neoplasia. 2007; 9:8–17. [PubMed: 17325739]

Farndale RW, Buttle DJ, Barrett AJ. Improved quantitation and discrimination of sulphated glycosaminoglycans by use of dimethylmethylene blue. Biochim Biophys Acta. 1986; 883:173–177. [PubMed: 3091074]

Farndale RW, Sayers CA, Barrett AJ. A direct spectrophotometric microassay for sulfated glycosaminoglycans in cartilage cultures. Connect Tissue Res. 1982; 9:247–248. [PubMed: 6215207]

Fermin CD, Lovett AE, Igarashi M, Dunner K Jr. Immunohistochemistry and histochemistry of the inner ear gelatinous membranes and statoconia of the chick (Gallus domesticus). Acta Anat (Basel). 1990; 138:75–83. [PubMed: 2368600]

Fisher LW, Fedarko NS. Six genes expressed in bones and teeth encode the current members of the SIBLING family of proteins. Connect Tissue Res. 2003; 44 Suppl 1:33–40. [PubMed: 12952171]

Fisher LW, Torchia DA, Fohr B, Young MF, Fedarko NS. Flexible structures of SIBLING proteins, bone sialoprotein, and osteopontin. Biochem Biophys Res Commun. 2001; 280:460–465. [PubMed: 11162539]

Fujisawa R, Wada Y, Nodasaka Y, Kuboki Y. Acidic amino acid-rich sequences as binding sites of osteonectin to hydroxyapatite crystals. Biochim Biophys Acta. 1996; 1292:53–60. [PubMed: 8547349]

Funderburgh JL. Keratan sulfate: structure, biosynthesis, and function. Glycobiology. 2000; 10:951–958. [PubMed: 11030741]

Girard JP, Springer TA. Modulation of endothelial cell adhesion by hevin, an acidic protein associated with high endothelial venules. J Biol Chem. 1996; 271:4511–4517. [PubMed: 8626806]

Hambrock HO, Nitsche DP, Hansen U, Bruckner P, Paulsson M, Maurer P, Hartmann U. SC1/hevin. An extracellular calcium-modulated protein that binds collagen I. J Biol Chem. 2003; 278:11351–11358. [PubMed: 12538579]

Hassell J, Yamada Y, rikawa-Hirasawa E. Role of perlecan in skeletal development and diseases. Glycoconj J. 2002; 19:263–267. [PubMed: 12975604]

He G, Dahl T, Veis A, George A. Nucleation of apatite crystals in vitro by self-assembled dentin matrix protein 1. Nat Mater. 2003; 2:552–558. [PubMed: 12872163]

He G, Gajjeraman S, Schultz D, Cookson D, Qin C, Butler WT, Hao J, George A. Spatially and temporally controlled biomineralization is facilitated by interaction between self-assembled dentin matrix protein 1 and calcium phosphate nuclei in solution. Biochemistry. 2005; 44:16140–16148. [PubMed: 16331974]

Hohenester E, Maurer P, Hohenadl C, Timpl R, Jansonius JN, Engel J. Structure of a novel extracellular Ca(2+)-binding module in BM-40. Nat Struct Biol. 1996; 3:67–73. [PubMed: 8548457]

Hohenester E, Maurer P, Timpl R. Crystal structure of a pair of follistatin-like and EF-hand calcium-binding domains in BM-40. EMBO J. 1997; 16:3778–3786. [PubMed: 9233787]

Hooft RW, Sander C, Scharf M, Vriend G. The PDBFINDER database: a summary of PDB, DSSP and HSSP information with added value. Comput Appl Biosci. 1996; 12:525–529. [PubMed: 9021272]

Hughes I, Saito M, Schlesinger PH, Ornitz DM. Otopetrin 1 activation by purinergic nucleotides regulates intracellular calcium. Proc Natl Acad Sci U S A. 2007; 104:12023–12028. [PubMed: 17606897]

Hunter GK, Kyle CL, Goldberg HA. Modulation of crystal formation by bone phosphoproteins: structural specificity of the osteopontin-mediated inhibition of hydroxyapatite formation. Biochem J. 1994; 300(Pt 3):723–728. [PubMed: 8010953]

Hurle B, Ignatova E, Massironi SM, Mashimo T, Rios X, Thalmann I, Thalmann R, Ornitz DM. Non-syndromic vestibular disorder with otoconial agenesis in tilted/mergulhador mice caused by mutations in otopetrin 1. Hum Mol Genet. 2003; 12:777–789. [PubMed: 12651873]

Ito S, Saito T, Amano K. In vitro apatite induction by osteopontin: interfacial energy for hydroxyapatite nucleation on osteopontin. J Biomed Mater Res A. 2004; 69:11–16. [PubMed: 14999746]

Jahnen-Dechent W, Schinke T, Trindl A, Muller-Esterl W, Sablitzky F, Kaiser S, Blessing M. Cloning and targeted deletion of the mouse fetuin gene. J Biol Chem. 1997; 272:31496–31503. [PubMed: 9395485]

Johnston IG, Paladino T, Gurd JW, Brown IR. Molecular cloning of SC1: a putative brain extracellular matrix glycoprotein showing partial similarity to osteonectin/BM40/SPARC. Neuron. 1990; 4:165–176. [PubMed: 1690015]

Jones SM, Erway LC, Bergstrom RA, Schimenti JC, Jones TA. Vestibular responses to linear acceleration are absent in otoconia-deficient C57BL/6JEi-het mice. Hear Res. 1999; 135:56–60. [PubMed: 10491954]

Jones SM, Erway LC, Johnson KR, Yu H, Jones TA. Gravity receptor function in mice with graded otoconial deficiencies. Hear Res. 2004; 191:34–40. [PubMed: 15109702]

Kang YJ, Stevenson AK, Yau PM, Kollmar R. Sparc protein is required for normal growth of zebrafish otoliths. J Assoc Res Otolaryngol. 2008; 9:436–451. [PubMed: 18784957]

Karita K, Nishizaki K, Nomiya S, Masuda Y. Calbindin and calmodulin localization in the developing vestibular organ of the musk shrew (Suncus murinus). Acta Otolaryngol Suppl. 1999; 540:16–21. [PubMed: 10445073]

Kawasaki K, Weiss KM. SCPP gene evolution and the dental mineralization continuum. J Dent Res. 2008; 87:520–531. [PubMed: 18502959]

Killick R, Legan PK, Malenczak C, Richardson GP. Molecular cloning of chick beta-tectorin, an extracellular matrix molecule of the inner ear. J Cell Biol. 1995; 129:535–547. [PubMed: 7721949]

Kiss PJ, Knisz J, Zhang Y, Baltrusaitis J, Sigmund CD, Thalmann R, Smith RJ, Verpy E, Banfi B. Inactivation of NADPH oxidase organizer 1 Results in Severe Imbalance. Curr Biol. 2006; 16:208–213. [PubMed: 16431374]

Knipper M, Richardson G, Mack A, Muller M, Goodyear R, Limberger A, Rohbock K, Kopschall I, Zenner HP, Zimmermann U. Thyroid hormone-deficient period prior to the onset of hearing is associated with reduced levels of beta-tectorin protein in the tectorial membrane: implication for hearing loss. J Biol Chem. 2001; 276:39046–39052. [PubMed: 11489885]

Krieger E, Koraimann G, Vriend G. Increasing the precision of comparative models with YASARA NOVA--a self-parameterizing force field. Proteins. 2002; 47:393–402. [PubMed: 11948792]

Landis WJ, Silver FH. Mineral deposition in the extracellular matrices of vertebrate tissues: identification of possible apatite nucleation sites on type I collagen. Cells Tissues Organs. 2009; 189:20–24. [PubMed: 18703872]

Legan PK, Lukashkina VA, Goodyear RJ, Kossi M, Russell IJ, Richardson GP. A targeted deletion in alpha-tectorin reveals that the tectorial membrane is required for the gain and timing of cochlear feedback. Neuron. 2000; 28:273–285. [PubMed: 11087000]

Legan PK, Rau A, Keen JN, Richardson GP. The mouse tectorins. Modular matrix proteins of the inner ear homologous to components of the sperm-egg adhesion system. J Biol Chem. 1997; 272:8791–8801. [PubMed: 9079715]

Lively S, Ringuette MJ, Brown IR. Localization of the extracellular matrix protein SC1 to synapses in the adult rat brain. Neurochem Res. 2007; 32:65–71. [PubMed: 17151913]

MacDougall M, Gu TT, Luan X, Simmons D, Chen J. Identification of a novel isoform of mouse dentin matrix protein 1: spatial expression in mineralized tissues. J Bone Miner Res. 1998; 13:422–431. [PubMed: 9525343]

Marcus DC, Wangemann P. Javier F, Alvarez-Leefmans ED. Cochlear and Vestibular Function and Dysfunction. Physiology and Pathology of Chloride Transporters and Channels in the Nervous System-From molecules to diseases. 2009:421–433.

Maurer P, Hohenadl C, Hohenester E, Gohring W, Timpl R, Engel J. The C-terminal portion of BM-40 (SPARC/osteonectin) is an autonomously folding and crystallisable domain that binds calcium and collagen IV. J Mol Biol. 1995; 253:347–357. [PubMed: 7563094]

McKinnon PJ, Margolskee RF. SC1: a marker for astrocytes in the adult rodent brain is upregulated during reactive astrocytosis. Brain Res. 1996; 709:27–36. [PubMed: 8869553]

McKinnon PJ, McLaughlin SK, Kapsetaki M, Margolskee RF. Extracellular matrix-associated protein Sc1 is not essential for mouse development. Mol Cell Biol. 2000; 20:656–660. [PubMed: 10611244]

Mendis DB, Brown IR. Expression of the gene encoding the extracellular matrix glycoprotein SPARC in the developing and adult mouse brain. Brain Res Mol Brain Res. 1994; 24:11–19. [PubMed: 7968348]

Mendis DB, Ivy GO, Brown IR. SC1, a brain extracellular matrix glycoprotein related to SPARC and follistatin, is expressed by rat cerebellar astrocytes following injury and during development. Brain Res. 1996a; 730:95–106. [PubMed: 8883893]

Mendis DB, Shahin S, Gurd JW, Brown IR. SC1, a SPARC-related glycoprotein, exhibits features of an ECM component in the developing and adult brain. Brain Res. 1996b; 713:53–63. [PubMed: 8724975]

Mothe AJ, Brown IR. Expression of mRNA encoding extracellular matrix glycoproteins SPARC and SC1 is temporally and spatially regulated in the developing cochlea of the rat inner ear. Hear Res. 2001b; 155:161–174. [PubMed: 11335086]

Mothe AJ, Brown IR. Differential mRNA expression of the related extracellular matrix glycoproteins SC1 and SPARC in the rat embryonic nervous system and skeletal structure. Brain Res. 2001a; 892:27–41. [PubMed: 11172746]

Murayama E, Herbomel P, Kawakami A, Takeda H, Nagasawa H. Otolith matrix proteins OMP-1 and Otolin-1 are necessary for normal otolith growth and their correct anchoring onto the sensory maculae. Mech Dev. 2005; 122:791–803. [PubMed: 15905077]

Murayama E, Okuno A, Ohira T, Takagi Y, Nagasawa H. Molecular cloning and expression of an otolith matrix protein cDNA from the rainbow trout, Oncorhynchus mykiss. Comp Biochem Physiol B Biochem Mol Biol. 2000; 126:511–520. [PubMed: 11026663]

Murayama E, Takagi Y, Nagasawa H. Immunohistochemical localization of two otolith matrix proteins in the otolith and inner ear of the rainbow trout, Oncorhynchus mykiss: comparative aspects between the adult inner ear and embryonic otocysts. Histochem Cell Biol. 2004; 121:155–166. [PubMed: 14689310]

Murayama E, Takagi Y, Ohira T, Davis JG, Greene MI, Nagasawa H. Fish otolith contains a unique structural protein, otolin-1. Eur J Biochem. 2002; 269:688–696. [PubMed: 11856329]

Murphy MB, Hartgerink JD, Goepferich A, Mikos AG. Synthesis and in vitro hydroxyapatite binding of peptides conjugated to calcium-binding moieties. Biomacromolecules. 2007; 8:2237–2243. [PubMed: 17530891]

Murshed M, Harmey D, Millan JL, McKee MD, Karsenty G. Unique coexpression in osteoblasts of broadly expressed genes accounts for the spatial restriction of ECM mineralization to bone. Genes Dev. 2005; 19:1093–1104. [PubMed: 15833911]

Paffenholz R, Bergstrom RA, Pasutto F, Wabnitz P, Munroe RJ, Jagla W, Heinzmann U, Marquardt A, Bareiss A, Laufs J, Russ A, Stumm G, Schimenti JC, Bergstrom DE. Vestibular defects in head-tilt mice result from mutations in Nox3, encoding an NADPH oxidase. Genes Dev. 2004; 18:486–491. [PubMed: 15014044]

Petko JA, Millimaki BB, Canfield VA, Riley BB, Levenson R. Otoc1: a novel otoconin-90 ortholog required for otolith mineralization in zebrafish. Dev Neurobiol. 2008; 68:209–222. [PubMed: 18000829]

Piscopo M, Avallone B, D'Angelo L, Fascio U, Balsamo G, Marmo F. Localization of calbindin D-28K in the otoconia of lizard Podarcis sicula. Hear Res. 2004; 189:76–82. [PubMed: 14987754]

Pollerberg GE, Mack TG. Cell adhesion molecule SC1/DMGRASP is expressed on growing axons of retina ganglion cells and is involved in mediating their extension on axons. Dev Biol. 1994; 165:670–687. [PubMed: 7958430]

Sage EH, Vernon RB. Regulation of angiogenesis by extracellular matrix: the growth and the glue. J Hypertens Suppl. 1994; 12:S145–S152. [PubMed: 7539492]

Sakagami M. Role of osteopontin in the rodent inner ear as revealed by in situ hybridization. Med Electron Microsc. 2000; 33:3–10. [PubMed: 11810451]

Salt AN, Inamura N, Thalmann R, Vora A. Calcium gradients in inner ear endolymph. Am J Otolaryngol. 1989; 10:371–375. [PubMed: 2596623]

Shapses SA, Cifuentes M, Spevak L, Chowdhury H, Brittingham J, Boskey AL, Denhardt DT. Osteopontin facilitates bone resorption, decreasing bone mineral crystallinity and content during calcium deficiency. Calcif Tissue Int. 2003; 73:86–92. [PubMed: 14506959]

Shen JW, Wu T, Wang Q, Pan HH. Molecular simulation of protein adsorption and desorption on hydroxyapatite surfaces. Biomaterials. 2008; 29:513–532. [PubMed: 17988731]

Soderling JA, Reed MJ, Corsa A, Sage EH. Cloning and expression of murine SC1, a gene product homologous to SPARC. J Histochem Cytochem. 1997; 45:823–835. [PubMed: 9199668]

Sollner C, Burghammer M, Busch-Nentwich E, Berger J, Schwarz H, Riekel C, Nicolson T. Control of crystal size and lattice formation by starmaker in otolith biomineralization. Science. 2003; 302:282–286. [PubMed: 14551434]

Sollner C, Schwarz H, Geisler R, Nicolson T. Mutated otopetrin 1 affects the genesis of otoliths and the localization of Starmaker in zebrafish. Dev Genes Evol. 2004; 214:582–590. [PubMed: 15480759]

Swartz DJ, Santi PA. Immunohistochemical localization of keratan sulfate in the chinchilla inner ear. Hear Res. 1997; 109:92–101. [PubMed: 9259239]

Sweetwyne MT, Brekken RA, Workman G, Bradshaw AD, Carbon J, Siadak AW, Murri C, Sage EH. Functional analysis of the matricellular protein SPARC with novel monoclonal antibodies. J Histochem Cytochem. 2004; 52:723–733. [PubMed: 15150281]

Takemura T, Sakagami M, Nakase T, Kubo T, Kitamura Y, Nomura S. Localization of osteopontin in the otoconial organs of adult rats. Hear Res. 1994; 79:99–104. [PubMed: 7806488]

Thalmann I, Hughes I, Tong BD, Ornitz DM, Thalmann R. Microscale analysis of proteins in inner ear tissues and fluids with emphasis on endolymphatic sac, otoconia, and organ of Corti. Electrophoresis. 2006; 27:1598–1608. [PubMed: 16609936]

Tohse H, Takagi Y, Nagasawa H. Identification of a novel matrix protein contained in a protein aggregate associated with collagen in fish otoliths. FEBS J. 2008; 275:2512–2523. [PubMed: 18410381]

Toyosawa S, Shintani S, Fujiwara T, Ooshima T, Sato A, Ijuhin N, Komori T. Dentin matrix protein 1 is predominantly expressed in chicken and rat osteocytes but not in osteoblasts. J Bone Miner Res. 2001; 16:2017–2026. [PubMed: 11697797]

Usami S, Shinkawa H, Inoue Y, Kanzaki J, Anniko M. Calbindin-D28K localization in the primate inner ear. ORL J Otorhinolaryngol Relat Spec. 1995; 57:94–99. [PubMed: 7731663]

Verpy E, Leibovici M, Petit C. Characterization of otoconin-95, the major protein of murine otoconia, provides insights into the formation of these inner ear biominerals. Proc Natl Acad Sci U S A. 1999; 96:529–534. [PubMed: 9892667]

Viviano BL, Silverstein L, Pflederer C, Paine-Saunders S, Mills K, Saunders S. Altered hematopoiesis in glypican-3-deficient mice results in decreased osteoclast differentiation and a delay in endochondral ossification. Dev Biol. 2005; 282:152–162. [PubMed: 15936336]

Wang Y, Kowalski PE, Thalmann I, Ornitz DM, Mager DL, Thalmann R. Otoconin-90, the mammalian otoconial matrix protein, contains two domains of homology to secretory phospholipase A2. Proc Natl Acad Sci U S A. 1998; 95:15345–15350. [PubMed: 9860971]

Wangemann P, Nakaya K, Wu T, Maganti RJ, Itza EM, Sanneman JD, Harbidge DG, Billings S, Marcus DC. Loss of cochlear HCO3- secretion causes deafness via endolymphatic acidification and inhibition of Ca2+ reabsorption in a Pendred syndrome mouse model. Am J Physiol Renal Physiol. 2007; 292:F1345–F1353. [PubMed: 17299139]

Wood JD, Muchinsky SJ, Filoteo AG, Penniston JT, Tempel BL. Low endolymph calcium concentrations in deafwaddler2J mice suggest that PMCA2 contributes to endolymph calcium maintenance. J Assoc Res Otolaryngol. 2004; 5:99–110. [PubMed: 15357414]

Xu T, Bianco P, Fisher LW, Longenecker G, Smith E, Goldstein S, Bonadio J, Boskey A, Heegaard AM, Sommer B, Satomura K, Dominguez P, Zhao C, Kulkarni AB, Robey PG, Young MF. Targeted disruption of the biglycan gene leads to an osteoporosis-like phenotype in mice. Nat Genet. 1998; 20:78–82. [PubMed: 9731537]

Yamakoshi Y, Hu JC, Fukae M, Iwata T, Kim JW, Zhang H, Simmer JP. Porcine dentin sialoprotein is a proteoglycan with glycosaminoglycan chains containing chondroitin 6-sulfate. J Biol Chem. 2005; 280:1552–1560. [PubMed: 15537641]

Young MF, Bi Y, Ameye L, Chen XD. Biglycan knockout mice: new models for musculoskeletal diseases. Glycoconj J. 2002; 19:257–262. [PubMed: 12975603]

Zhao X, Jones SM, Thoreson WB, Lundberg YW. Osteopontin is not critical for otoconia formation or balance function. J Assoc Res Otolaryngol. 2008a; 9:191–201. [PubMed: 18459000]

Zhao X, Jones SM, Yamoah EN, Lundberg YW. Otoconin-90 deletion leads to imbalance but normal hearing: a comparison with other otoconia mutants. Neuroscience. 2008b; 153:289–299. [PubMed: 18355969]

Zhao X, Yang H, Yamoah EN, Lundberg YW. Gene targeting reveals the role of Oc90 as the essential organizer of the otoconial organic matrix. Dev Biol. 2007; 304:508–524. [PubMed: 17300776]

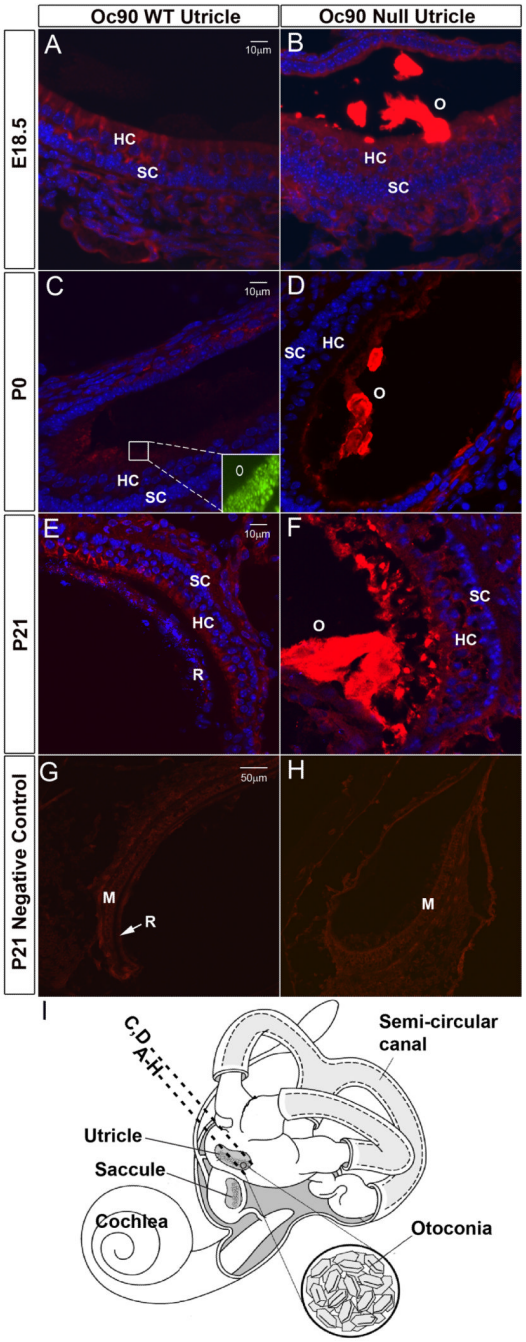

Figure 1.

Deposition of Sc1 in Oc90 wt and null otoconia (the utricle is shown). Immunostaining is shown in (**A, B**) E18.5, (**C, D**) P0, (**E, F**) P21 and (**G, H**, negative controls at P21 using non-immune serum). In (**A**, **C**, **E**), WT otoconia had extremely faint staining that was slightly visible only under the microscope but not in the photographs, whereas the giant crystals (labeled as “O” in B, D, F) in null tissues were intensely stained. Inset in C shows the presence of normal otoconia in the wt tissue section as detected by Oc90 immunostaining. (**I**) An illustration of the mouse inner ear. The dashed line labeled with A–H shows the approximate location of the sections except C, D, which are located more periphery as

marked by the dashed line above. All epithelial cell types in the utricle and saccule participate in otoconia formation. HC, hair cells; SC, supporting cells; M, macula; R, roof.

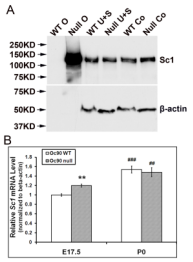

Figure 2.

Otoconial deposition and cellular expression of Sc1 in Oc90 wt and null vestibules. (**A**) Western blotting of Sc1 in Oc90 wt and null tissues. 6 μg total protein from Oc90 wt otoconia (labeled as “WT O”), 2 μg total protein from null otoconia (“Null O”), and 20 μg total protein from each of the epithelial cellular extracts (U, utricle; S, saccule; Co, cochlea) were loaded. In Oc90 wt otoconia, there was only a faint band after a long exposure; whereas a large amount of Sc1 was detected in Oc90 null otoconia (age P2–3). The same membrane was stripped and re-used for β-actin. β-actin is not present in otoconia, but the equal amount of β-actin detected in each epithelial extract shows that the micro-BCA assay accurately measured the protein content, which was used to control the loading amount. (**B**) Real-time PCR shows a small but significant increase in *Sc1* mRNA in the Oc90 null utricular and saccular epithelia as compared to wt tissues at age E17.5 (**, $P<0.01$, n=3) but not at P0 (n=3). The relative *Sc1* expression levels are higher at P0 than E17.5 in both genotypes (## and ###, $P<0.01$ and $P<0.001$, respectively, P0 vs. E17.5 within the same genotype).

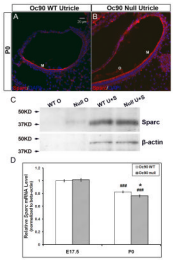

Figure 3.

Deposition of Sparc in Oc90 wt and null otoconia and its cellular expression (the utricle is shown). Immunostaining is shown in (**A, B**) P0. Negative controls are similar to Figure 1. WT otoconia show no visible staining, but the giant crystals ("O") in null tissues are mildly stained. HC, hair cells; SC, supporting cells. (**C**) Western blotting of Sparc in Oc90 wt and null tissues. Otoconia extracts with equal total protein show a small amount of Sparc in the null otoconia that is absent in wt otoconia (age P15, 7 μg each). The cellular Sparc level is similar between wt and null tissues (20 μg total protein was loaded for each). The same membrane was stripped and re-used for β-actin. β-actin is not present in otoconia, but the equal amount of β-actin detected in each epithelial extract shows that the micro-BCA assay accurately measured the protein content, which was used to control the loading amount. (**D**) Real-time PCR shows no significant difference in *Sparc* mRNA levels between wt and null utricular and saccular epithelia at age E17.5 and a small difference at age P0 (* indicates $P<0.05$, n=4). Expression reduces with age for both genotypes (###, $P<0.001$, P0 vs. E17.5 within the same genotype).

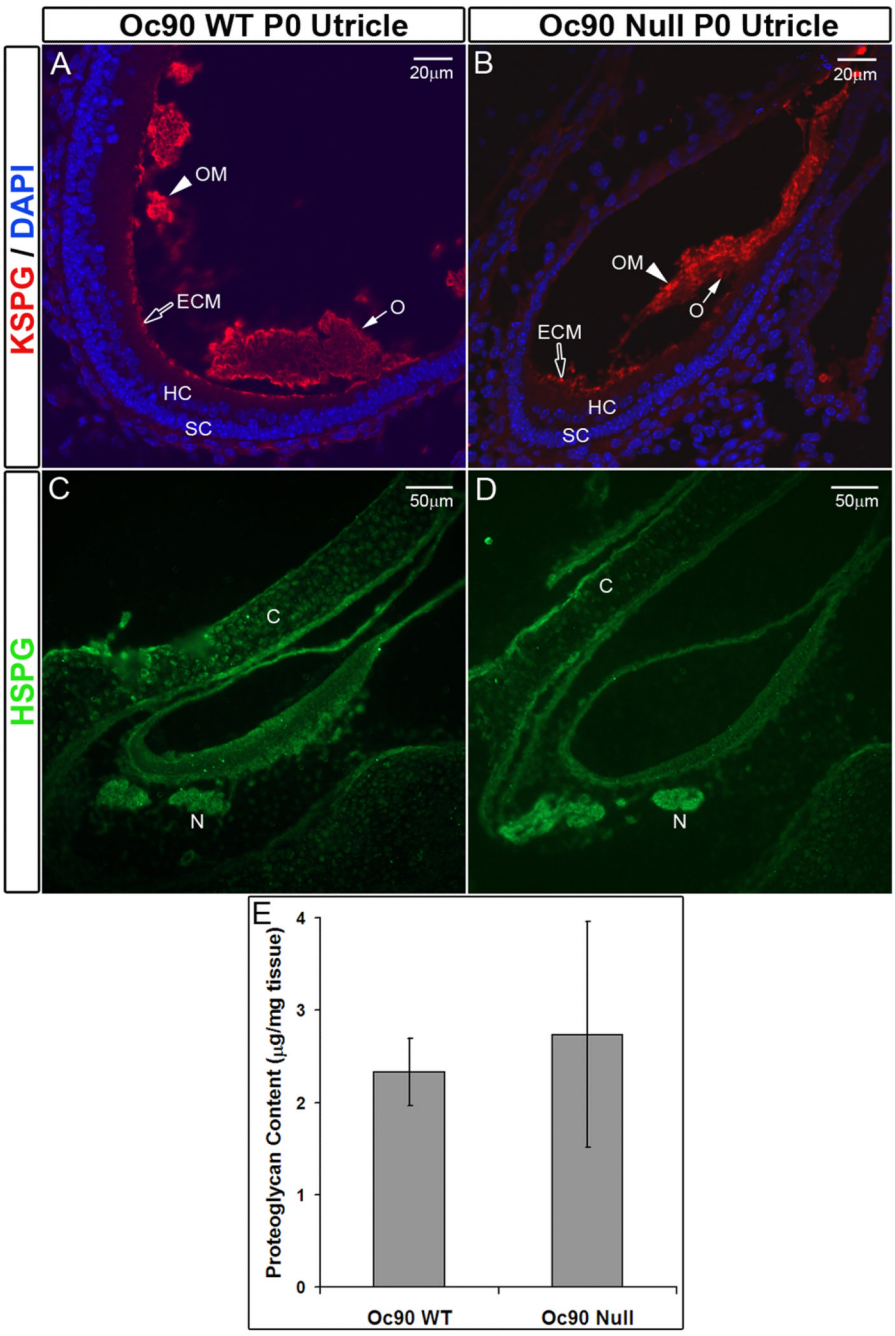

Figure 4.

Presence of KSPG (**A, B**) and absence of HSPG (**C, D**) in murine otoconia. (**E**) DMB proteoglycan assay shows no significant difference in the total epithelial proteoglycan content between Oc90 wt and null utricles and saccules (n=4, P=0.2, age P6). C, cartilage; ECM, extra-cellular matrix; HC, hair cells; M, macula; N, nerve fiber; O, otoconia; OM, otoconial membrane; SC, supporting cells.

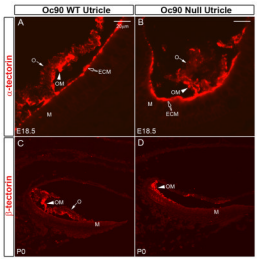

Figure 5.

Presence/absence of α-tectorin (**A, B**) and β-tectorin (**C, D**) in murine otoconia. Expression and deposition of these proteins are not affected in the Oc90 null vestibule. The tectorins are abundant in the extra-cellular matrix (ECM) and otoconial membrane (OM). There is an occasional staining of α-tectorin in the wt crystals. ECM, extracellular matriz; M, Macula; O, otoconia; OM, otoconial membrane.

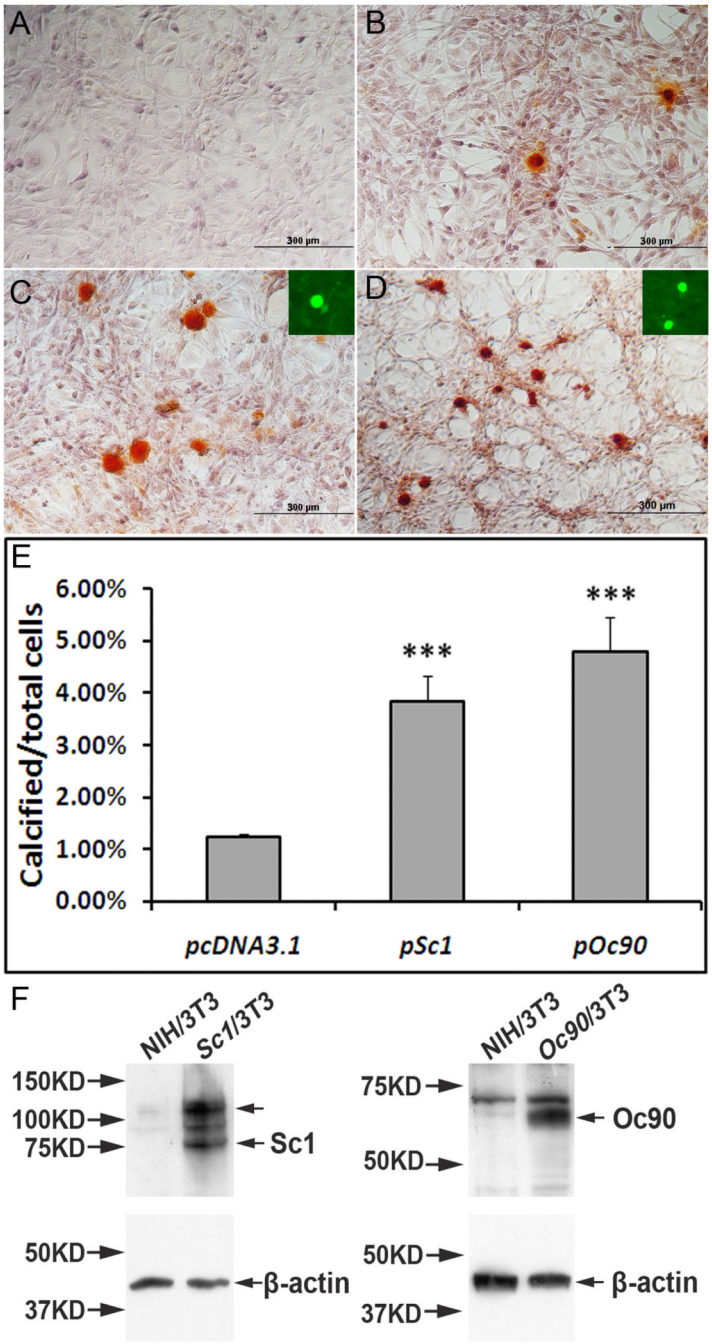

Figure 6.

The effects of Oc90 or Sc1 on ECM calcification. NIH/3T3 cells stably transfected with (**C**) pSc1 and (**D**) pOc90 calcified intensely after 5 days of induction with 0.5 mM Ca^{2+} and 2mM Pi. Inorganic calcium deposits were visualized with ARS staining, proteins with fluorescent immunostaining. Averaged percentages of cells with ECM calcification over total cells were compared for different vectors. Under the same culture conditions, untransfected cells and cells transfected with empty vectors (pcDNA3.1 is shown in **B**) had similar ratios of calcification, but both had significantly lower ratios than those transfected with Oc90 or Sc1 (Figure 6C & 6D vs. 6B, $p<0.001$, n=3 experiments × 3~4 survey fields in each). Insets in C & D show that Sc1 and Oc90, respectively, are present in the calcified

nodules. Figure 6E shows histograms of the averaged percentages of cells with ECM calcification. No calcification was seen in cells transfected with any of these constructs and cultured under standard media without supplemental Ca^{2+} and Pi (**A**). (**E**) Western blotting of Sc1 and Oc90 in untransfected and transfected cells. 20 μg total protein was loaded in each lane. Each membrane was stripped and re-used for β-actin detection. The upper arrow in the Sc1 lane corresponds to Sc1 dimer in the size of ~130–140 kD.

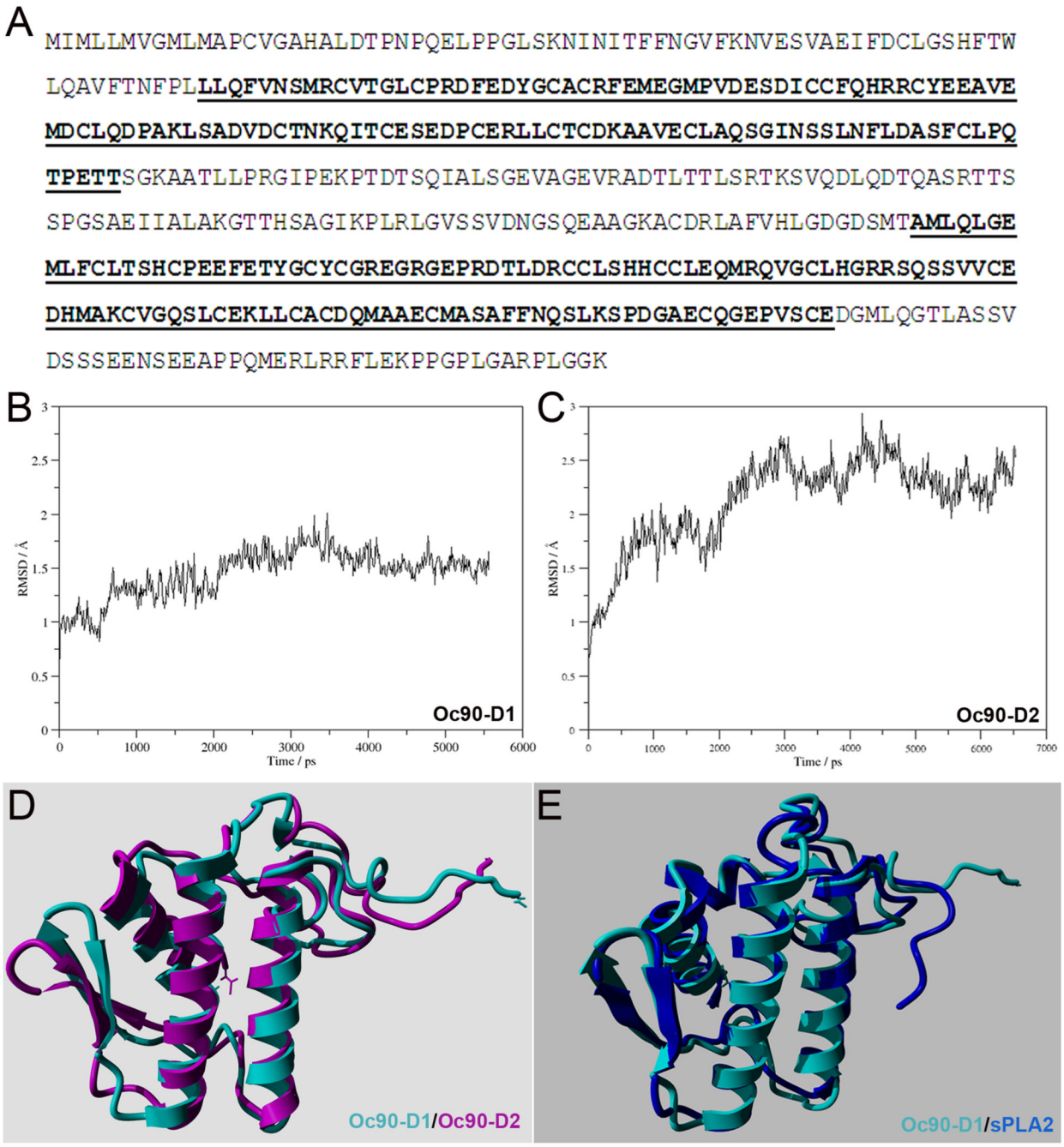

Figure 7.

(**A**) Amino acid sequence of murine Oc90 (Swiss-Prot id Q9Z0L3). The Pla2l domains are underlined and bolded. (**B, C**) Backbone RMSD of the first 102 residues as function of simulation time of Oc90-D1 and -D2 (the 1st and 2nd Pla2l domain, respectively). (**D**) Overlaid time-averaged structures of Oc90-D1 (cyan) and -D2 (purple). (**E**) Overlaid structures of Oc90-D1 (cyan) and human sPLA2 (blue). The RMSD of the two overlaid structures is 1.517 Å, indicating high structural similarity.

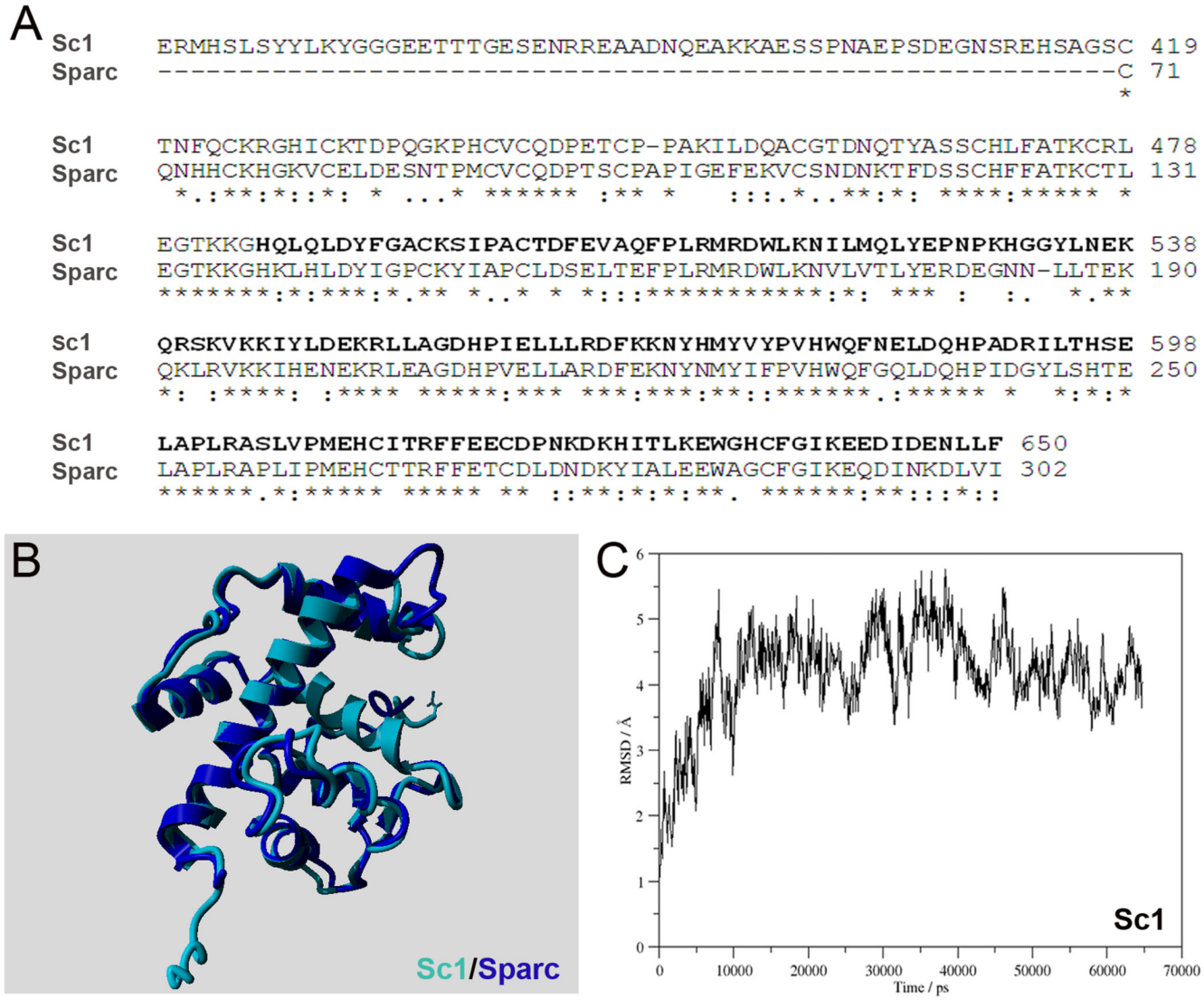

Figure 8.

(**A**) Alignment of the sequences of murine Sc1 (Swiss-Prot id P70663) and murine Sparc (Swiss-Prot id P07214). Residues 489 to 650, for which the homology model was built, are underlined and bolded. (**B**) Overlaid structures of Sc1 (489–650) (purple) and the known crystal structure of the collagen- and Ca^{2+}-binding domain of human SPARC (blue). The RMSD is 1.023 Å, indicating high structural similarity. (**C**) Backbone RMSD of Sc1 as function of simulation time.

Table 1

Antibodies used in the present study.

Antibody name	Immunogen	Host species	Final concentration		Supplier	Recognized protein size
			IHC	WB		
Sc1 (polyclonal)	NS0-derived rmSC1 (aa 17–650)	Goat	1:100 (2ng/ul)	1:500 (0.4ng/ul)	R&D	72KD
Sparc (polyclonal)	NS0-derived rm Sparc	Goat	1:100 (1ng/ul)	1:500 (0.2ng/ul)	R&D	35KD
KSPG (monoclonal)	Hu articular cartilage proteoglycan	Mouse	1:200		Chemicon	425KD
HSPG (monoclonal)	Mammals	Mouse	1:50 (0.02ug/ul)		Chemicon	64KD
HSPG (monoclonal)	HSPG from EHS mouse tumor	Rat	1:50		Chemicon	>400KD
α-tectorin (polyclonal)	Chick α-tectorin (α1-subunit)	Rabbit	1:400		Dr. Richardson	239KD
β-tectorin (polyclonal)	Chick β-tectorin	Rabbit	1:200		Dr. Richardson	37KD
β-actin (monoclonal)	*β-actin (aa 1–14)	Mouse		1:1000 (3.1ng/ul)	Sigma	42KD
β-actin (polyclonal)	Hu β-actin (aa 1–100)	Goat		1:1000 (1.4ng/ul)	Abcam	42KD

rm, rat mouse; hu, human;

* peptide common in many species (mammals, birds and lower vertebrates)

Table 2

Otoconia/otolith component proteins identified to date. Bolded ones are identified and validated in the present study.

	Presence in Otoconia	Otoconia phenotype	References
Mouse	Otoconin-90 (Oc90)	Giant otoconia	Zhao et al., 2007
	Otolin-1	---	---
	Osteopontin	Normal otoconia	Zhao et al., 2008
	Fetuin-A	Normal otoconia?	Zhao et al., 2007; Thalmann et al., 2006
	Sparc-like 1 (Sc1)	---	---
	Sparc	---	---
	KSPG	---	---
	DMP1	---	---
	α-tectorin	Reduced otoconia layer	Legan et al., 2000
Fish	Otolith matrix protein	Residual seeding	Murayama et al., 2004
	Otolin-1	Fused, unstable	Murayama et al., 2004
	Starmaker	Inorganic, calcite	Sollner et al., 2003
	Sparc	Small otoliths	Kang et al,, 2008
	Otoc1 (zOc90)	Small otoliths	Petko et al,, 2008
	Matrix macromolecule-64	---	---
	Precerebellin-like (Cbln1)	---	---
	Neuroserpin	---	---

---, no mutant available or unknown otoconia/otolith phenotype.